Asia-Pac. J. Atmos. Sci., 50(3), 283-296, 2014
DOI:10.1007/s13143-014-0017-6

pISSN 1976-7633 / eISSN 1976-7951

The Implementation of Reverse Kessler Warm Rain Scheme for Radar Reflectivity Assimilation Using a Nudging Approach in New Zealand

Sijin Zhang, Geoff Austin, and Luke Sutherland-Stacey

Atmospheric Physics Group, The University of Auckland, Auckland, New Zealand

(Manuscript received 21 August 2013; accepted 7 November 2013)

Abstract: Reverse Kessler warm rain processes were implemented within the Weather Research and Forecasting Model (WRF) and coupled with a Newtonian relaxation, or nudging technique designed to improve quantitative precipitation forecasting (QPF) in New Zealand by making use of observed radar reflectivity and modest computing facilities. One of the reasons for developing such a scheme, rather than using 4D-Var for example, is that radar VAR scheme in general, and 4D-Var in particular, requires computational resources beyond the capability of most university groups and indeed some national forecasting centres of small countries like New Zealand. The new scheme adjusts the model water vapor mixing ratio profiles based on observed reflectivity at each time step within an assimilation time window. The whole scheme can be divided into following steps: (i) The radar reflectivity is firstly converted to rain water, and (ii) then the rain water is used to derive cloud water content according to the reverse Kessler scheme; (iii) The cloud water content associated water vapor mixing ratio is then calculated based on the saturation adjustment processes; (iv) Finally the adjusted water vapor is nudged into the model and the model background is updated. 13 rainfall cases which occurred in the summer of 2011/2012 in New Zealand were used to evaluate the new scheme, different forecast scores were calculated and showed that the new scheme was able to improve precipitation forecasts on average up to around 7 hours ahead depending on different verification thresholds.

Key words: Nudging, assimilation, radar reflectivity, precipitation, warm rain

1. Introduction

Quantitative precipitation forecasting (QPF) plays an important role in both meteorological and hydrological risk management. However, probably largely due to the inaccuracy of initial fields and the associated "spin-up" problem, QPF does not usually produce results of high accuracy. It is to be hoped that improved data assimilation will be able to improve initial backgrounds and thus significantly improve QPF on short term scale. Weather radar networks, like the one operated in New Zealand by MetService Ltd. (NZ MetService) (Crouch, 2003), are able to provide very high spatial and temporal resolution rainfall observations and the availability of such data allows the use of radar reflectivity and Doppler velocity to initialize models with better precipitation fields.

There are various approaches for assimilating radar observation in NWP models for QPF. These approaches usually have different target variables to adjust, different effective periods and different computational resources demands. The variational (VAR) technique have been implemented to assimilate variety types of observations, including radar reflectivity and Doppler velocity (e.g., Xiao *et al*., 2002; Barker *et al*., 2004; Huang *et al*., 2009; Barker *et al*., 2012). Encouraging results have shown that it can be effective to assimilate radar data for mesoscale NWP (e.g., 4D-Var radar data assimilation experiments described by Sun and Wang (2013)). However, the performance of VAR is affected by a number of constraints in the cost function (e.g., the continuity, the reflectivity conservation and spatial smoothness) (Sun, 2005) and the availability of large computation resources (e.g., the calculations of 4D-Var, are usually performed at a coarser grid than that which the model is actually run, which can be much coarser than the radar observation, due to the expensive computational demand (e.g., Sokol and Zacharov, 2012)). Another limitation of VAR is the assumption of Gaussian error distribution (Dance, 2004). Moreover, in the current version of Weather Research and Forecasting (WRF) model 3D-Var radar data assimilation system, the linearization error of the existing reflectivity assimilation operator may cause the difficulty in convergence of a cost function when the background rainwater is very small (Sun and Crook, 1997; Wang *et al*., 2013a).

The Ensemble Kalman Filter (EnKF) is another method, which has a demonstrated potential for incorporating radar data into models (Sun, 2005) and may require less computational resources compared to 4D-Var depending on number of ensemble members and resolution (e.g., Snyder and Zhang, 2003; Zhang, *et al*., 2004). Caya *et al*. (2005) found that the EnKF scheme performed less well than 4D-Var in the first two cycles (by using 4D-Var Doppler Radar Analysis System (VDRAS) and simulated radar data) while the techniques had comparable performance thereafter. Moreover, from an operational viewpoint, the number of members for the EnKF must be limited, which influences the accuracy of the error characteristics and consequently the accuracy of the forecast would be compromised correspondingly (Sokol and Zacharov, 2012).

An alternative simple technique - nudging, which is set up

Corresponding Author: Sijin Zhang, Physics Department, the University of Auckland, Room 724, The Science Centre, Building 303, 38 Princes Street, Auckland, New Zealand.
E-mail: szha226@aucklanduni.ac.nz

based on an algorithm in which the model is set equal to observed values, presented the potential for assimilating radar observations at high resolution but with less computational cost (e.g., Stauffer and Seaman, 1990, 1994; Stephan *et al*., 2008; Dixon *et al*., 2009) . The application of nudging is often carried out on the (very) short-range precipitation forecasts operationally because the computational demands of the 4D-Var and EnKF methods (Sokol and Zacharov, 2012). For precipitation nudging, a widely used scheme is the "latent heat" (LHN) method which was firstly designed by Manobianco *et al.* (1994). Similar approaches have been developed and implemented in the UK Met. Office Mesoscale Model (Jones and Macpherson, 1997) and the Bologna Limited Area Model (BOLAM) (Davolio and Buzzi, 2004). The LHN rescales model latent heat profiles by the ratio of derived surface rain rates and model precipitation and it has been proven to be an effective method in improving precipitating in the first few hours of forecast. Another alternative idea, which is usually referred as physical initialization (PI), was developed based on the assumption that updrafts associated with horizontal humidity flux convergence in the lower part of the cloudy column lead to rain formation. This scheme was first investigated in tropical regions (Krishnamurti *et al*., 1991), the satellite observed rainfall rates and vertically integrated radiative heating rates were used to diagnose the surface fluxes of water vapor and sensible heat, and a reverse cumulus parameterization algorithm was employed to analyse the humidity variables according to the imposed precipitation rates. Outgoing longwave radiation (OLR) matching was used to improve the model cloud cover distributions. Similar algorithms were developed and implemented by Nunes and Cocke (2004) in a regional spectral model over South America. For radar reflectivity PI, Haase *et al*. (2000) developed a method (Physical Initialization Bonn (PIB)) adjusting the model vertical wind using a simplified precipitation mechanism and assigning relevant specific water vapor and cloud water according to the vertical distributions of cloud (In this scheme, the cloud top is estimated from satellite or using 3D radar observation (Yang *et al*., 2006) and cloud base height is set to lifting condensation level (LCL) derived from synoptic observation). Another simple but effective reflectivity assimilation approach by nudging is the Water Vapor Correction (WVC) method (Sokol and Rezacova, 2009). By using the empirical relationship between water content and reflectivity obtained from two Joss-Waldvogel disdrometers located at Locarno-Monti, Swizerland during the Mesoscale Alpine Programme (MAP) (Hagen and Yuter, 2003), this method was tested using the Local Model (LM) COSMO (Stephan *et al*., 2008) in Czech Republic (CR) and results showed that the WVC method was able to successfully improve the LM forecasts of CR significantly in short range forecasts of precipitation.

For assimilating radar reflectivity observation in WRF with modest computational resources, this paper presents an alternative method for radar assimilation other than the WRF VAR direct radar assimilation system (avoiding the linearization error of the current WRF 3DVar direct radar reflectivity assimilation (Wang *et al*., 2013a) and expensive computational demands). The new scheme is inspired by the WVC technique and the idea of Krishnamurti *et al*. (1991), and based on reversing the Kessler warm rain processes (RK-nudging) (Kessler, 1969). In the new scheme, the target nudging water vapor is obtained from the usual Kessler warm rain processes and corresponding saturation adjustments in reverse order: (rain water $q_r \rightarrow$ cloud water $q_c \rightarrow$ water vapor q_v). Overall, the principle of this method is similar to the LHN and WVC approaches, which are standard options for some operational model systems like the Unified Model (UM) and COSMO model, as the precipitation is increased or decreased by adding (removing) water vapour flux into (from) the model backgrounds. The adjustment (releasing/absorbing) of heat could be caused by oversaturation or undersaturation after the corrections of water vapour and then at subsequent model integration steps, the corresponding phase changes and relevant effects on the heat balance may be implicated.

However, in the LHN method, the potential temperature increments are based on a scaling of the profiles of R_{obs}/R_{bk}, where R_{obs} indicates the observed rain rate (or the analysed rain rate which is a weighted combination of the observed rain rate) and R_{bk} represents the model background (or "first guess") rain rate. It is apparent that this will not work when the background is "dry" ($R_{bk} = 0$). One approach to address this issue is "borrowing" the moisture-related fields from the nearest "wet" grid point, but clearly it might introduce significant errors, especially when we try to trigger isolated cell which is far away from the main rain band. Therefore, in comparison of the LHN method, the new scheme can be implemented in the "dry" model background though a physical rather than mathematical argument. Moreover, in contrast to the radar reflectivity PI approach, the RK-nudging scheme has the capability of processing 3D radar volume scanning information without the estimation of cloud distributions (e.g., cloud top and bottom height) before the assimilation using other types of observations (e.g., satellite and synoptic observations). In addition, the new approach, which is set up based on the well tested Kessler warm rain scheme, does not require the coefficients which have to be determined over a large number of cases studies as is necessary in the WVC approach. Thus, the RK-nudging method has the potential to be straightforwardly implemented in different regions for different types of precipitation.

The processes of adjusting the model backgrounds in WRF by the RK-nudging scheme can be described as: (i) the assimilation scheme starts by adjusting the model water vapor mixing ratio: the derived rain rate $q_{r\text{-}radar}$ from reflectivity is used to calculate the corresponding cloud water increments Δq_c, and then Δq_c is converted to the water vapor mixing ratio. At this step, all required intermediate variables are obtained from existing model states. (ii) After the temporal and spatial linear interpolations, the increments of water vapor is nudged into model and used to adjust the original model state (In real applications, we found that, by the appropriate spatial linear

smoothing of the target radar reflectivity data before nudging, it appeared that the assimilation process could be speeded up due to smoother data being incorporated. Although the effects were trivial for most cases and it risks the loss of small structures in observed precipitation patterns, it still could be helpful that if there are only very limited computational resources available). (iii) at the subsequent integration time step, the adjusted water vapor is applied to diagnose precipitation fields (e.g., cloud and rain water) according to the usual formulations of the Kessler warm rain scheme.

The paper is divided into 5 sections: the section 2 introduces the RK-nudging algorithm. The evaluation of 13 cases which occurred in the summer of 2011/2012 in New Zealand by the RK-nudging is presented in Section 3. Discussions and conclusions are given in Section 4 and Section 5, respectively.

2. The RK-nudging assimilation scheme

"Warm rain" refers to rain derived from clouds without ice-phase processes. Warm rain can be considered as a relative simple, but integral component of precipitation system (e.g., Lau and Wu, 2003) as its capability of effective adjusting moistening and heating in a convection system. The Kessler scheme (Kessler, 1969) presents a very simple warm rain parameterization which is still widely used today (e.g., Ogura and Takahashi, 1973; Dudhia, 1989; Schultz, 1995). In this paper, the Kessler scheme has been reversed (RK) in order to adjust the model profile of water vapor mixing ratio according to observed radar reflectivity. In the RK-nudging scheme, the increments of rain water mixing ratio between radar derivations and model backgrounds are assumed to be entirely resulted from the autoconversion, accretion and evaporation processes. Most moisture related states, except rain water, cloud water and water vapor, are updated by the model dynamical and physical processes themselves according to the adjusted water vapor at subsequent time steps. The orographic effects, which present in most regions of New Zealand, especially in the South Island, can provide the forced upward motion for the RK scheme after the saturation adjustment. There are mainly four steps to implement the RK nudging scheme into model:

(i) Firstly, the rain water mixing ratio associated with radar observed reflectivity is determined according to the reversed $Z - q_r$ relationship (Sun and Crook, 1997):

$$q_{r-radar} = \frac{1}{\rho} 10^{Z-c_1/c_2}, \tag{1}$$

where Z is the reflectivity in dBZ, ρ is the air density and $q_{r\text{-}radar}$ indicates the rain water mixing ratio derived from radar. c_1 and c_2 are constants equal to 43.1 and 17.5, respectively. This equation is also employed as the nonlinear observation operator H for WRF 3D-Var direct radar reflectivity assimilation system, and the performance of this equation as H has been investigated in detail by Wang *et al*. (2013a).

(ii) The difference between model rain water and radar derived rain water can be represented as:

$$\Delta q_r = q_{r\text{-}radar} - q_r . \tag{2}$$

Therefore, if $\Delta q_r > 0$ (the model rain water is underestimated), we assume that the increments of rain water are entirely defined by the increments of cloud water, thus following equation can be symbolically used to approximate the Δq_r producing processes:

$$\Delta q_r = A_r(\Delta q_c) + C_r(q_r, \Delta q_c) - E_r, \tag{3}$$

where A_r, C_r and E_r represent autoconversion, accretion and evaporation, respectively. q_r is model rain content. Δq_c is used to represent the changes of cloud water leading the rain water adjustments. The different terms of above equation are given by (Kessler, 1969; Klemp and Wilhelmson, 1978):

$$A_r(\Delta q_c) = k_1(\Delta q_c - a), \tag{4}$$

$$C_r(\Delta q_c, q_r) = k_2(\Delta q_c) q_r^c, \tag{5}$$

$$E_r = \frac{1}{\overline{\rho}} \frac{C(1 - q_v/q_{vs})(\overline{\rho} q_r)^{0.525}}{5.4 \times 10^5 + 2.55 \times 10^6 / p q_{vs}}, \tag{6}$$

where k_1, k_2 and a are all constants and in this paper they have been selected as: $k_1 = 0.001\ s^{-1}$, k_2=2.2 s^{-1}, $a = 0.001\ gg^{-1}$. C is the ventilation factor. q_v, q_r and q_{vs} are water vapour, rain water and saturation mixing ratio, respectively, and $\overline{\rho}$ and p represent density of air and pressure, respectively. Thus, the increments of cloud water can be simply represented as:

$$\Delta q_c = \max\left[\frac{\Delta q_r + k_1 a + E_r}{k_1 + k_2 q_r^c}, 0.0\right]. \tag{7}$$

(iii) The conversion between cloud water and water vapor in this procedure is defined by the saturation adjustment described by Soong and Ogura (1973) and Klemp and Wilhelmson (1978). In contrast to the values after the saturation adjustment (q_v and q_{vs}), the dummy values which only take into account the dynamical terms in the model prognostic equations for water vapor and saturation mixing ratio are represented by q_v^* and q_{vs}^*, respectively. If $q_v^* > q_{vs}^*$, the air is oversaturated while it is not permitted in the model. Thus, the original oversaturated water vapor (q_v^*) is adjusted to $q_v = q_v^* - r(q_v^* - q_{vs}^*)$ with $r = [1 + \{237 a \pi_e q_{vs}^* / (\pi_e \theta^* - 36)^2\}(L/C_p \overline{\pi})]^{-1}$. Considering the conservation equation $q_v + q_c = q_v^* + q_c^*$ (Klemp and Wilhelmson, 1978), the increments of water vapor in the RK-nudging therefore can be written as:

$$\Delta q_v = \max\left[\frac{\Delta q_c}{r} - q_v + q_{vs}, 0.0\right], \tag{8}$$

where π_e is the non-dimensional pressure, $a = 17.2694$ and θ^* is the potential temperature before the adjustment. In $\overline{\pi} = \pi_e + \Delta\pi/2$, $\Delta\pi$ is the non-dimensional pressure difference between two levels that the air is in the moist adiabatic process.

Similarity, if $\Delta q_r < 0$ (the model rain water is overestimated), Δq_c and Δq_v can be addressed using a similar form of

Table 1. Selected cases and the associated daily accumulated rainfall (mm) observed by NIWA/NZ MetService.

Case number	Date (dd/mm/yy)	Daily accumulated rainfall (mm)							
		Auckland	Whangarei	Rotorua	Wellington	Nelson	Christchurch	Queenstown	Invercargill
1	01/11/2011	10.3	14.5	---	---	12.7	---	---	---
2	09/11/2011	1.0	0.6	0.8	13.6	5.5	15.2	0.2	0.0
3	20/11/2011	0.0	0.0	0.0	1.8	0.2	7.4	18.8	11.6
4	21/11/2011	0.2	0.0	0.2	0.8	0.2	15.4	2.8	0.0
5	04/12/2011	---	3.6	0.4	---	---	0.0	0.0	0.0
6	15/12/2011	19.8	3.6	19.4	11.6	38.6	21.4	3.8	0.2
7	29/12/2011	29.8	12.5	12.6	9.6	47.2	0.0	0.0	0.0
8	30/12/2011	36.8	12.5	68.6	43.2	28.6	1.2	0.0	0.0
9	31/12/2011	7.2	30.0	68.4	16.0	0.2	0.6	0.0	0.0
10	07/01/2012	26	---	63.2	3.6	0.0	0.2	0.0	0.0
11	08/01/2012	4.4	---	11.8	39.6	1.5	2.6	0.0	0.0
12	12/01/2012	4.6	3.2	8.8	7.2	7.0	8.0	10.2	23.9
13	13/01/2012	0.4	0.0	0.2	0.0	0.0	0.2	19.6	25.1

Eqs. (7)-(8), the only different is to keep Δq_c and Δq_v less than (or at least equal to) zero in the nudging processes.

$$\Delta q_c = \min\left[\frac{\Delta q_r + k_1 a + E_r}{k_1 + k_2 q_r^c}, 0.0\right], \quad (9)$$

$$\Delta q_v = \min\left[\frac{\Delta q_c}{r} - q_v + q_{vs}, 0.0\right]. \quad (10)$$

(iv) Finally, Δq_v is used to adjust the model background water vapor mixing ratio using the WRF Obs-nudging system (Liu *et al*., 2005). The nudging factor was selected to 3×10^{-4} s^{-1} for all cases in order to keep the model stability and still give the priority to the model physical and dynamical processes during the integration processes (Stauffer and Seaman, 1989). The horizontal influential radius was given to 3.0 km, which is equal to the model spatial resolution. It is helpful to keep the model stability as the effects of assimilation would not be too widespread and each grid point was determined largely by the most closely adjacent observed value. The vertical influential radius (η) was set to 0.1 as this value is a reasonable value suggested by WRF User's Guide. Considering that we just made a one-time nudging and no phase error was considered, a short temporal influential radius was set (30 min).

It is worthwhile to mention that, the entire data assimilation scheme is set up according to the liquid only microphysics scheme, which may cause errors in the assimilation of heavy rainfall event. Detailed analysis for the limitation of the scheme can be found in Section 4.

3. Results and discussions

In this section, the evaluations of the assimilation scheme with a selection of 13 cases were drawn from the summer of 2011/2012 (between November 2011 and January 2012). Synoptic analyses (not shown) indicate that most of these events either resulted from moist air masses developing in the Tasman Sea or were generated locally by the orographic impacts of South Alps, which mean that these 13 cases have covered most common precipitation generation mechanisms that occur during a NZ summer. The daily accumulated rainfall observed by NZ National Institute of Water and Atmosphere Research (NIWA) / MetService of these 13 cases are presented in Table 1.

Currently, NZ MetService runs seven Doppler C-band radars at Auckland (AKL), Bay of Plenty (BOP), Christchurch (CNY), Invercargill (INV), Mahurangi (MAH), Napier (NPL) and Willington (WLG). There are additional two radars due for installation by the end of 2013. The spatial resolution of the radars is range-dependent from about 150 m to a few kilometres and around 7 minutes in time with 7 levels, which is sufficient to characterise most types of precipitation. The scan covers an area out to a range of about 480 kilometres. The national radar network not only covers all metropolitan areas and most coast regions of New Zealand, it also provides limited offshore forecast ability that extending the high resolution observations to the maximum about 200 km out of the coast.

All cases were initialized using previous 6 h free forecasts from WRF (the free forecasts were initialized with NCEP $1^o \times 1^o$ Final Analysis Data) as in the operational configuration of the MetService system, most models are updated four times a day (It is worth noting that, currently, synoptic observations are assimilated into the MetService system operationally, thus, the results shown in this study, which with only radar reflectivity assimilated, may be slightly different from the expected one obtained from the future operational application). Observed reflectivity from the NZ MetService radars was incorporated at 0000 for the Da runs (as Fig. 1. In this paper, we did not update the backgrounds continuously with nudging since the main purpose of this paper is investigating the "immediate"

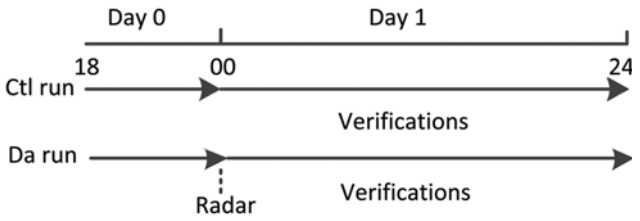

Fig. 1. Experimental designs for all selected cases. Ctl run: initialized with only previous 6 h free forecasts at 0000 UTC; Da run: initialized with radar reflectivity and previous 6 h forecasts at 0000 UTC.

response of WRF from the one time RK-nudging scheme process). The errors associated with phase changes were not considered in this paper, but it is worthwhile to mention that, within the 30 min of time window, there might be significant changes in the precipitation distribution and intensity. For example, in Fig. 2, the precipitation located in the west coast of New Plymouth was apparently strengthened from (T+0) to (T+30min). Errors might be caused if we use the (T+0) observed reflectivity to represent the characteristics of precipitation over the entire 30 min.

The model was configured with two domains (Fig. 3), the outer domain (D01) covers the Tasman Sea with the horizontal grid resolution of 9 km, and the inner domain (D02) covers New Zealand and the surrounding waters at 3-km grid spacing. This configuration was established considering both the current available computational resources and the operational demands in New Zealand (at current stage, the highest resolution of all models run by the NZ MetService is lower than 3 km). The model physics options adopted in this paper include: the Kessler scheme was adopted for microphysics processes. Other parameterizations used include the Rapid Radiative Transfer Model (RRTM) scheme (Mlawer *et al*., 1997) for long wave radiation and the Dudhia scheme (Dudhia, 1989) for short wave radiation, the Yonsei University (YSU) scheme (Noh *et al*., 2003) for planetary boundary layer parameterization. The verifications were starting from 0100 UTC. One hour model rainfall accumulations were verified against one hour radar derived rainfall accumulations (radar data were spatially averaged to 3 km) in terms of different thresholds. The hourly radar rainfall accumulation is estimated using an advection

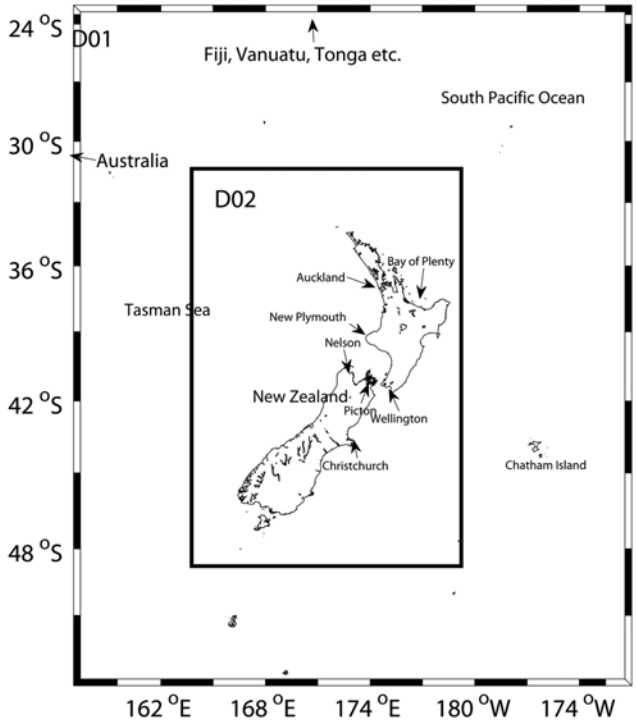

Fig. 3. Model outer domain (D01) and inner domain (D02) adopted in this study. The spatial resolutions for D01 and D02 are 9 km and 3 km, respectively.

based interpolation scheme (Fabry *et al*., 1994; Shucksmith *et al*., 2011).

The forecasts were evaluated objectively using both point wise and fuzzy verification schemes in the region covered by radars. Firstly, Equitable Threat Score (ETS) and False Alarm Ratio (FAR) were calculated by comparing radar observations and forecasts point by point. ETS aims to show that how well the model predicted precipitation corresponds to observations. It is ranged between 0 to 1: 0 indicates no skill and 1 indicates prefect forecast. FAR shows the fraction of forecasted events for which the event actually does not occur. It is also ranged from 0 to 1 while 0 indicates perfect skill and 1 indicates no skill. Secondly, a fuzzy verification method ~ Fractions Skill Score (FSS) (Roberts and Lean, 2008) is used. FSS is well

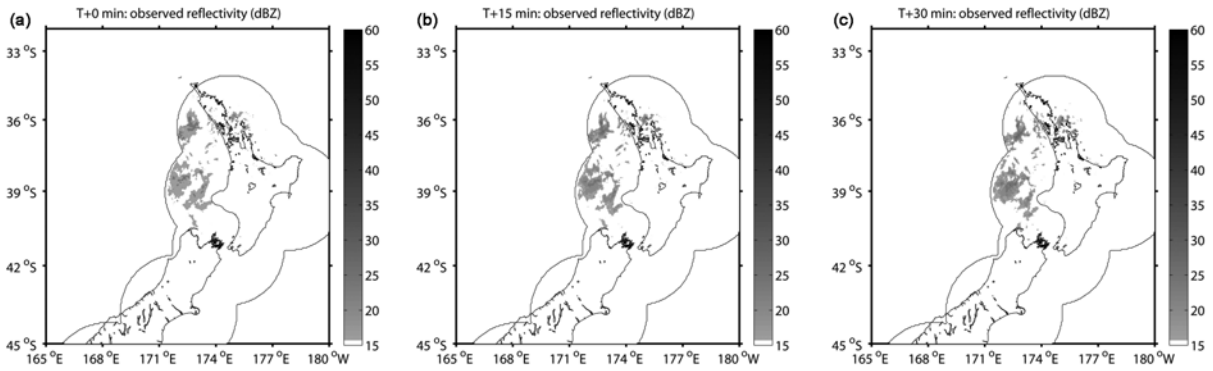

Fig. 2. Phase changes of radar observed reflectivity (dBZ) at 0000 UTC (T+0) , 0015 UTC (T+15min) and 0030 UTC (T+30min) 1 November 2011.

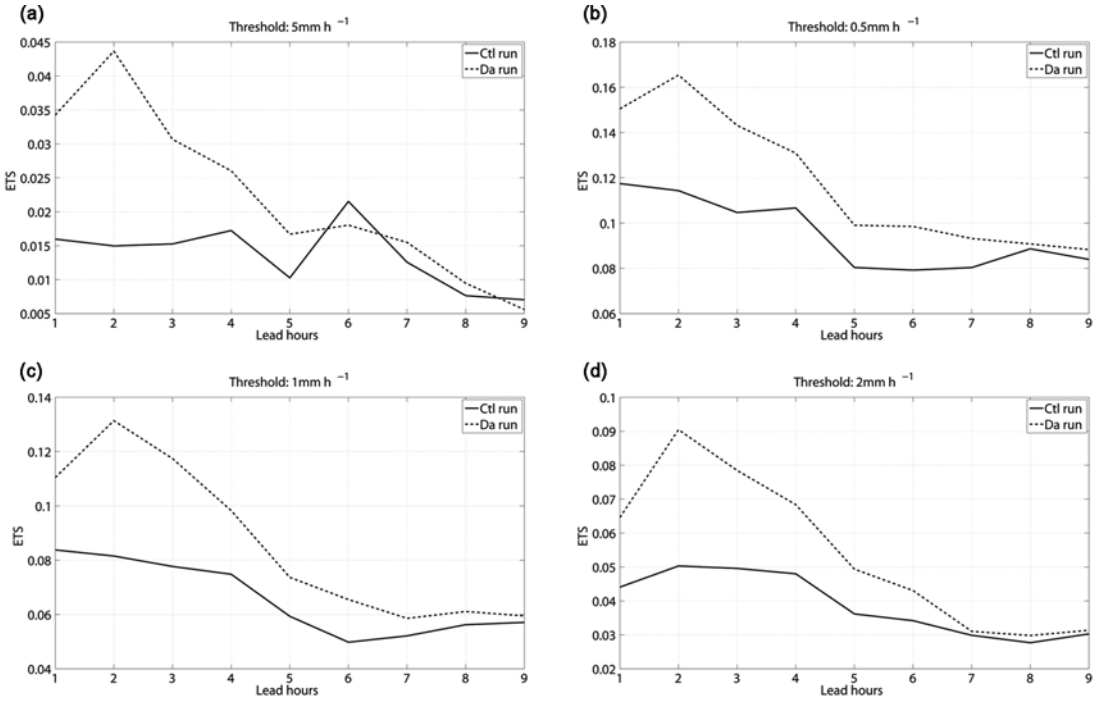

Fig. 4. Mean ETS scores in terms of different thresholds and lead hours. Horizontal axis indicates forecast lead hours and vertical axis indicates the average scores. Verification thresholds: 0.5 mm h^{-1} (top-left), 1.0 mm h^{-1} (top-right), 2 mm h^{-1} (bottom-left) and 5 mm h^{-1} (bottom-right).

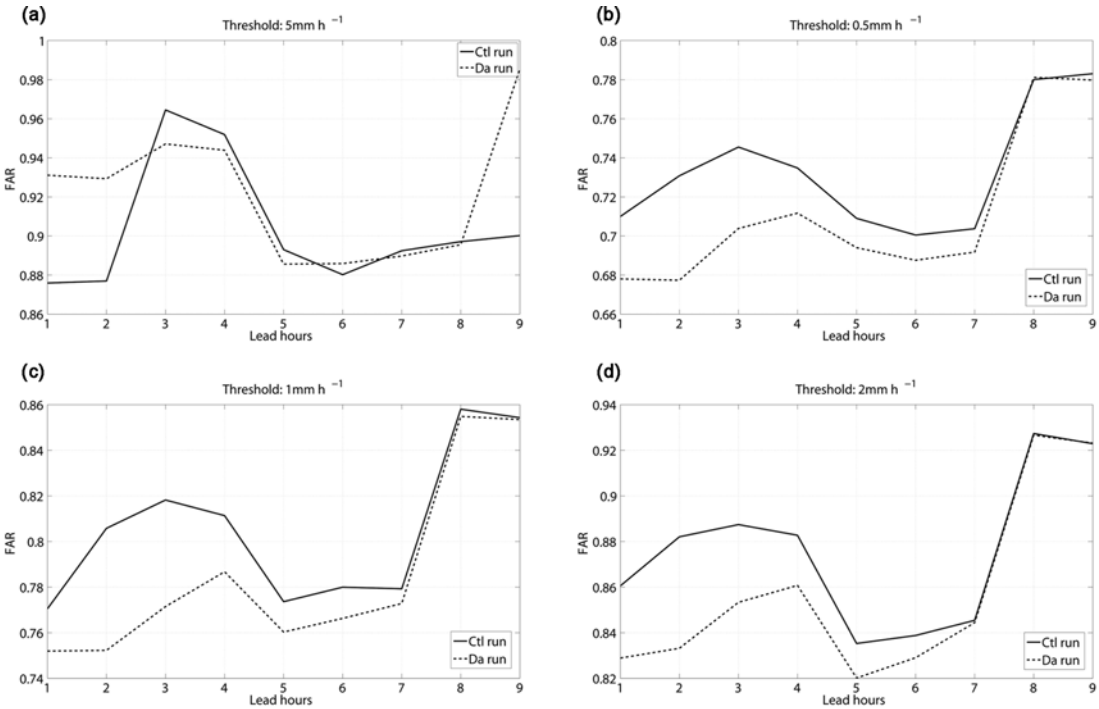

Fig. 5. Same as Fig. 4 but with FAR scores.

suitable for discontinuous fields (e.g., precipitation) and can be used to compare forecasts at different spatial scales. FSS ranges between 0 (completely wrong forecast) and 1 (prefect forecast) as above. It is worth noting that all of these scores are largely determined by given thresholds, and it is difficult to determine if the forecast was useful by using any types of objective evaluation scores (e.g., setting up an empirical threshold), however, these scores provide an easy way to compare

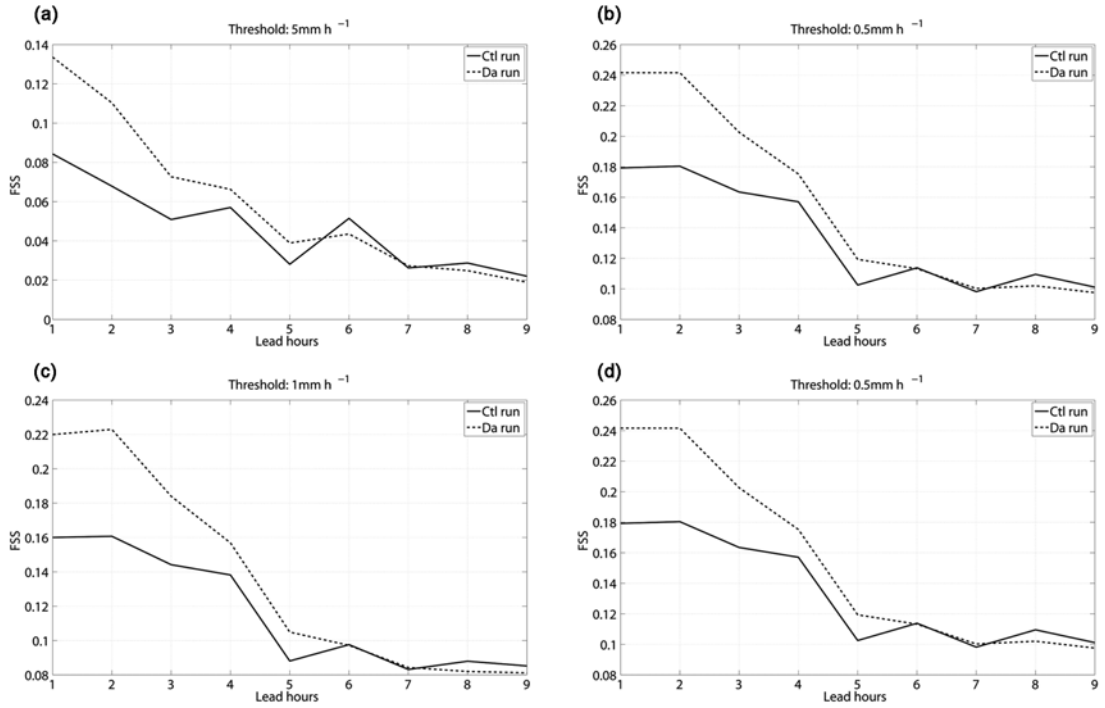

Fig. 6. Same as Fig. 4 but with FSS scores (the verification scale is 10 km).

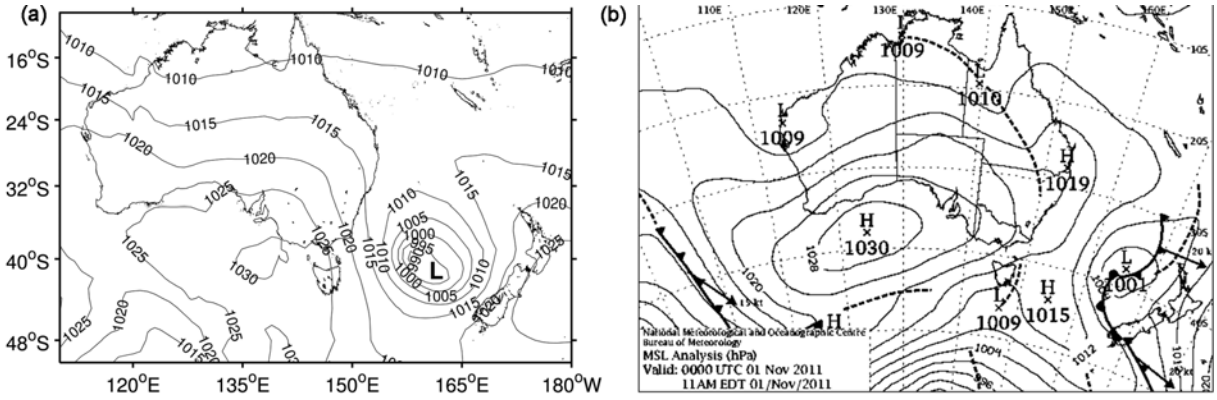

Fig. 7. MSLP analysis (Manual) obtained from Bureau of Meteorology, Australia (top) and the associated WRF simulated MSLP analysis (bottom) at 0000 UTC 1 November 2011.

the relative skill of different forecast approaches or the capability of same forecast scheme over a certain period (Rossa *et al*., 2008; Gilleland *et al*., 2010).

Scores were averaged over all selected cases in terms of different thresholds (0.5 mm h^{-1}, 1.0 mm h^{-1}, 2.0 mm h^{-1} and 5.0 mm h^{-1}) and shown in Fig. 4 (ETS statistics), Fig. 5 (FAR statistics) and Fig. 6 (FSS statistics corresponding to the verification scale of 10 km). From these three figures, we can clearly see that the RK-nudging scheme was able to improve the precipitation forecasts significantly, especially for the first 2 hours. When the threshold was set to above 2.0 mm h^{-1}, the forecast skills for both the Ctl and Da experiments were very low, which means that the assimilation scheme was still not capable of capturing relatively intense precipitation. The impacts of assimilation reduced gradually with the lead hours increasing, the positive effects led by the RK-nudging could endure up to around 7 hours (by ETS and FAR) and 6 hours (by FSS). After that, the difference between the Ctl runs and Da runs were not obvious. From the FAR scores, we can easily find that when the threshold was set to 5.0 mm h^{-1}, the assimilation clearly increased the false alarm ratio during the first few hours. There are several plausible reasons for that, it might be, perhaps, that there was spurious high intensity precipitation wrongly produced by the assimilation, and when using skill scores to evaluate the forecasts, the wrong precipitation prediction introduced by the nudging processes could not be offset by its ability of reducing false warnings in other places when the threshold became high.

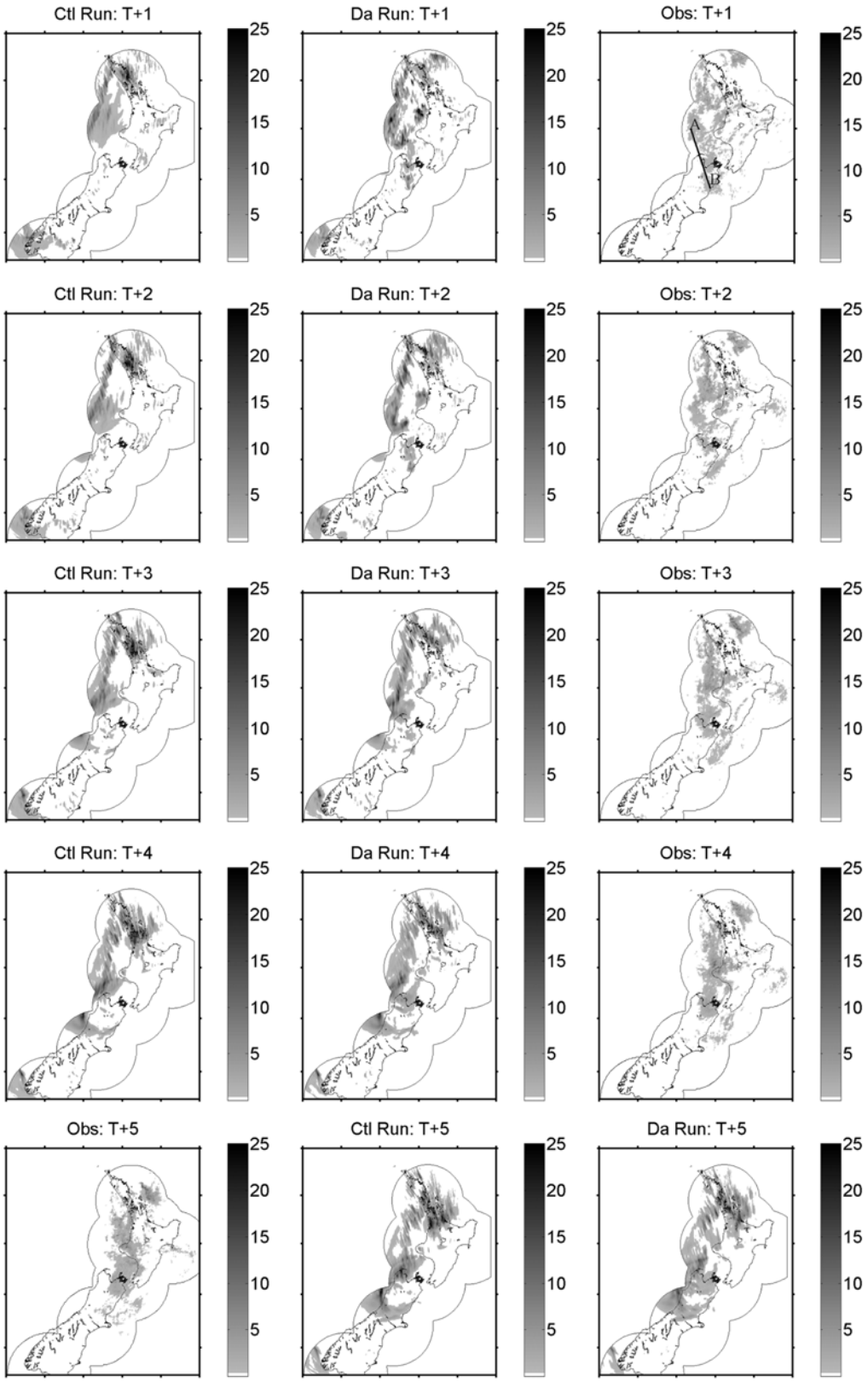

Fig. 8. Hourly accumulated precipitation (mm) for the case of 1 November 2011 at 0100 UTC (T+1), 0200 UTC (T+2), 0300 UTC (T+3), 0400 UTC (T+4) and 0500 UTC (T+5). Ctl run (left column), Da run (middle column) and the associated radar observations (right column) are plotted with the threshold of 0.05 mm h^{-1}. A-B indicates the position of the vertical cross section shown in Fig. 9.

It is worthwhile to make that, from all above statistical scores, the skills of the Da runs followed the similar trend as the Ctl runs. For example, high Ctl based scores are usually associated with high Da based scores and poor Ctl forecasts also came with poor performance of the assimilation experiments. This indicates that even when observations have been incorporated into the model using the RK-nudging scheme, the forecast skills were still largely determined by the model dynamical and physical processes and simulated synoptic situations (e.g., if the model could provide correct simulation of synoptic analysis). Figure 7 gives the difference of low pressure centers (LPC) from manually produced Mean Sea Level Pressure (MSLP) analysis obtained from the Bureau of Meteorology, Australia and the associated WRF simulated MSLP analysis. From Fig. 7, it is obvious that the WRF simulated LPC located on the southwest of the manually analyzed one, which could result the wrong simulated location of the main precipitation band. Apparently, the water vapor adjustment in this case (Fig. 8) was not enough to correct the pressure system sufficiently and subsequently made significant changes to the precipitation development. The results are similar to Sokol (2009) which suggested that sometimes the nudging based radar reflectivity assimilation alone is too weak to adjust the state of the model variables then does not support the development of convective activity, and in such case, the assimilation of satellite data or wind fields may provide more fundamental impacts on the predicted precipitation development.

Subjective assessments of each case were carried out and the results showed that the RK-nudging can give considerable benefit in increasing precipitation areas in accord with radar observations, while it has only slight improvements on reducing false precipitation warnings. We present an example of subjective examination for the case of 1 November 2011 (Fig. 8). From 31 October to 2 November 2011, isolated rain bands developed in the Tasman Sea and affected NZ. Resulting heavy rainfalls led to numerous hazards like flooding and landslides across the country, especially in the North Island. The radars operated by NZ MetService detected strong echoes from around 2300 UTC 31 October, and then the echoes moved rapidly eastwardly and passed out of the radar range after about 18 hours. The maximum reported reflectivity (over 50 dBZ from 0000 to 1200 UTC) was recorded in some regions (e.g., Bay of Plenty) in the North Island and the top of the South Island (from Picton to Nelson region).

Figure 8 gives the comparisons from 0100 UTC (30 minutes after the end of assimilation time window) between the forecasts and observations. The results without (Ctl) and with (Da) radar adjustments are shown at the left and middle column, respectively. Associated radar observations are shown at the right column.

At 0100 UTC, the Ctl run did not predict the precipitation in the Nelson/Tasman region at all while the Da run showed the rain band well in this region but with higher intensity in general. There were isolated light - moderate rainfalls observed in the central of the North Island where neither experiment provided very good simulations. Spurious rainfall areas predicted by the Ctl run were decreased by the assimilation processes used in the bottom of the South Island. Generally, the Da run showed much higher ability to forecast the rainfall distributions compared to the Ctl run, but both experiments overestimated the intensity of rainfall in most places.

One hour later (0200 UTC), similar to 0100 UTC, the main rain bands simulated by the Ctl were still located in the west of NZ and had almost has no impact on the North Island except the Northland region. The Ctl run was still not able to produce clear precipitation in the Nelson/Tasman region although approximately 5 mm h^{-1} rainfalls were already presented in the observations. In contrast, the Da run produced an isolated rain cell along the west coast of the North Island and also, there were rainfalls presented at the top of the South Island (Nelson/Tasman region). However, similarity to the Ctl run, the main rain band simulated by the Da was still located in the west of the North Island.

The difference between the Da and Ctl runs decreased as the forecast lead time increases. At 0400 UTC (3 hours after the end of assimilation), both experiments were failed to provide satisfactory predictions in the North Island. Spurious echoes were produced by both experiments in the Central South Island. However, compared to the observations, the Da provided better simulations in the Tasman region. Moreover, the forecasts by the Da run were more realistic in the top of the North Island compared to the Ctl run.

At 0500 UTC, The Ctl and Da runs provided very similar results in the North Island. However, the Da run presented a border precipitation area in the region of New Plymouth, which is more realistic compared to the associated observations. Moreover, the rain band affected the South Island already moved across Picton and the Da run provided better forecasts in the region.

Figure 9 shows the vertical cross section (the position of the vertical cross-section is shown in Fig. 8) of simulated rain water (shaded) and vertical winds (solid contour). It is apparent that, from (172.00, −39.00) to (172.48, −40.12), where precipitation is mostly over the sea, the vertical winds have been adjusted by the model physical and dynamical prognostic formulae after the assimilation processes by adding/removing water vapor. In contrast, updraft and rain water also can be strengthened by topography as in the position from (173.2, −41.8) to (173.44, −42.36), the north section of the South Alps. Overall, the combination of adjusted water vapor and the topography would lead to the adjusted updraft, which could have significant effects on the moisture related fields development in the target analysis region.

Generally, for the event of 1 November 2011, the Da run, which with the observed reflectivity adjustments, was able to provide higher forecast skills on average compared to the Ctl run by visually evaluation. However, compared to the associated observations, both experiments (Ctl and Da) overestimated the maximum intensity of rainfall significantly at the beginning although with the lead time increasing, the simulated

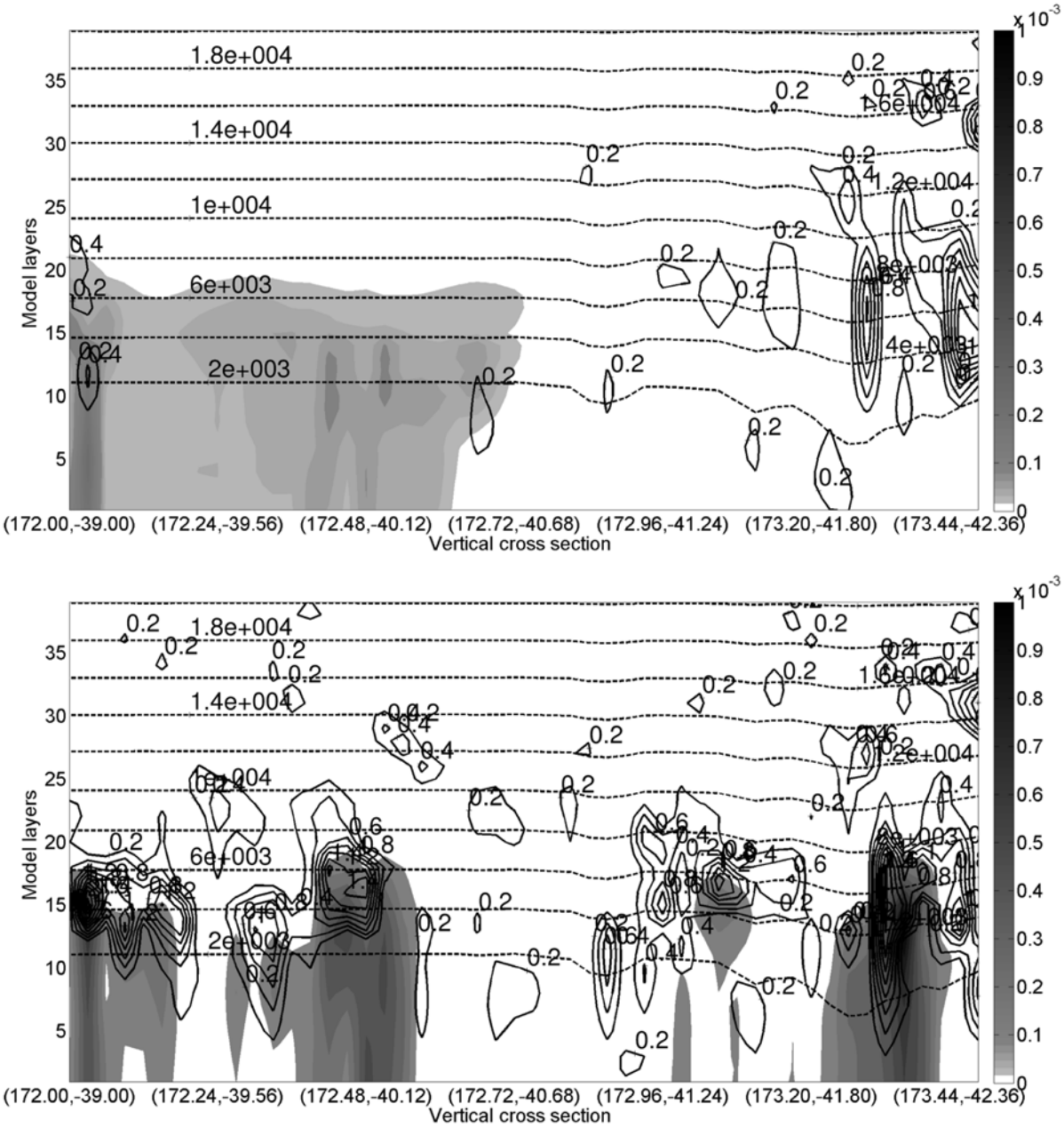

Fig. 9. Vertical cross section (the position of the vertical cross-section is shown in Fig. 8) of simulated rain water (kg kg^{-1}) (shaded) and vertical winds (m s^{-1}) (in black solid contour) at 0100 UTC 1 November 2011 for the Ctl run (top) and the Da run (bottom). Black dot contour indicates the height (m) at each model level.

intensity became more reasonable. Moreover, the accumulated rainfall patterns were not improved apparently as the main simulated rain band from the Da run was still located at the west side of the corresponding observations on average, especially after 1-2 hours. This shows that the assimilation of wind fields from Doppler velocity might provide much better precipitation forecasts for this case. Therefore, the future New Zealand radar data assimilation scheme should be the implementation of both the reflectivity and winds operators. In WRF, there is no linear approximation errors existing in the Doppler velocity assimilation system, thus, by using the WRF direct radar assimilation system, the wind assimilation, in most cases, is capable of providing more positive effects on the precipitation forecasts compared to the assimilation of reflectivity data (e.g., Xiao *et al*., 2005). Therefore, a method similar to the WRF Variational wind assimilation approach is expected to be employed at next step but by using the nudging technique for the incorporation of observed Doppler velocity in New Zealand.

Figure 10 gives the statistics of maximum rain water vapor (calculated from the column bottom to top at each grid point within the radar coverage) distributions at (T+1), which was 30

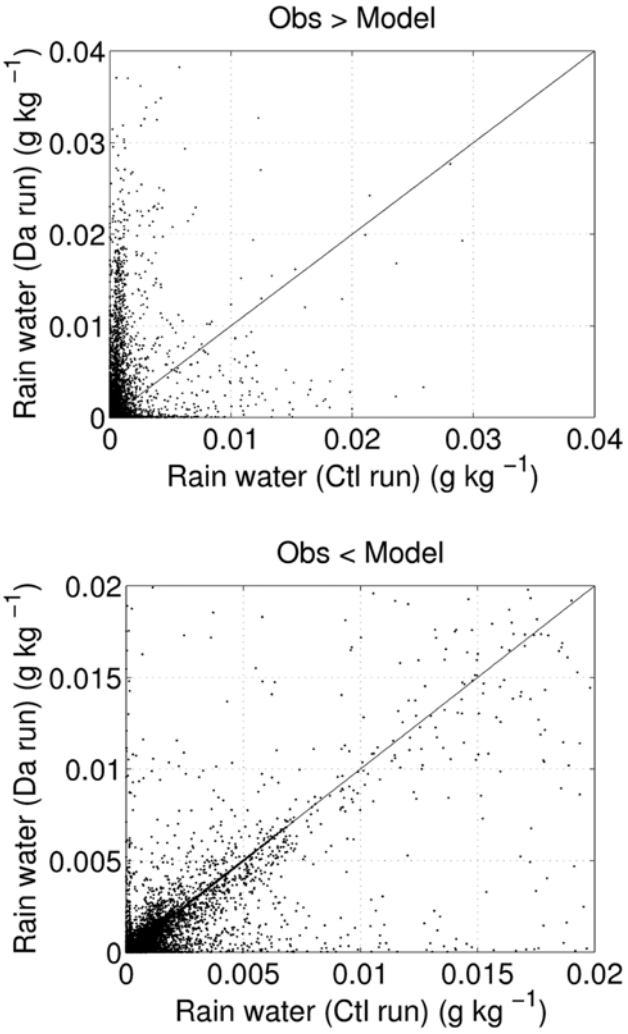

Fig. 10. The distributions of maximum rain water (g kg^{-1}) for the Ctl run (horizontal axis) and Da run (vertical axis) at (T+1), which was 30 minutes after the end of the obs-nudging time window. Top: it shows the situation where assimilated radar derived rain water was larger than the model backgrounds at (T+0). Bottom: shows the opposite situation where the assimilated derived rain water was smaller than the model backgrounds at (T+0).

minutes after the end of the nudging time window. Horizontal and vertical axes indicate the values from the Ctl run and Da run, respectively, for the case of 1 November 2011. It is obvious that, regardless of whether higher or lower values were assimilated, the nudging scheme and the model physical and dynamical processes might drive the expected result the opposite way: for example, the assimilation of lower radar derived rain water value (compared to the model backgrounds) could result higher output after the assimilation processes. However, for most grid points, when the higher (lower) radar reflectivity was assimilated to a relative dryer (wetter) grid point, the model background value could be increased (decreased) accordingly. Moreover, from the figure, the performance of the RK-nudging on increasing rain water was clearly better than the capability of decreasing rain water, which was

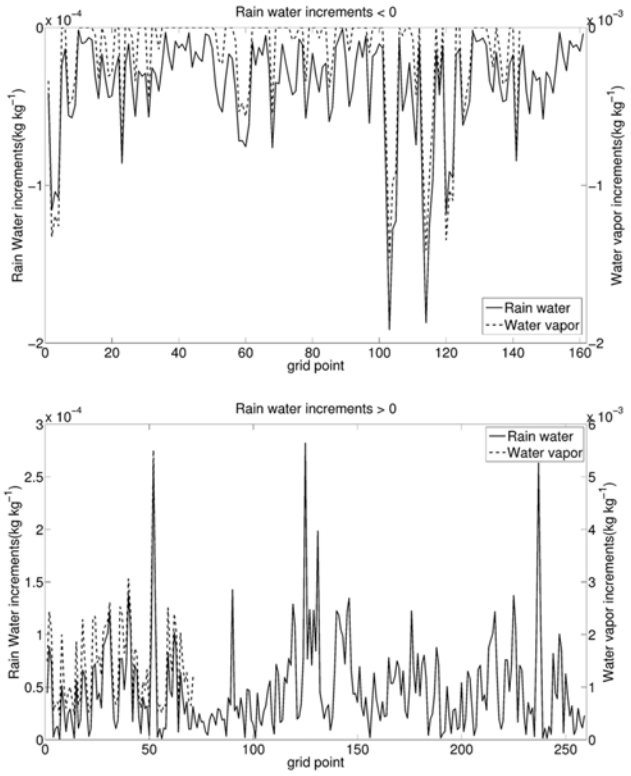

Fig. 11. The comparisons between Δq_v and the corresponding Δq_r at 0000 UTC 1 November 2011 (Δq_v and Δq_r were calculated by the reverse Kessler scheme but have not been assimilated into the model by nudging approach). Top: $\Delta q_r > 0$. Bottom: $\Delta q_r < 0$.

agreement with the subjective evaluations for most other cases selected in this paper.

The comparisons between Δq_v and the corresponding Δq_r for the event before the nudging processes (Δq_v and Δq_r were calculated by the reverse Kessler scheme but have not been assimilated into the model by nudging approach) are shown in Fig. 11. Apparently, for both the situations that $\Delta q_r > 0$ (observed rain water is larger than the model rain water) and $\Delta q_r < 0$ (observed rain water is less than the model rain water), the RK process was capable of responding appropriately on average. For $\Delta q_r > 0$, the associated Δq_v is usually larger than zero as well and the model water vapor is expected to be increased by the subsequent nudging processes. In contrast, when $\Delta q_r < 0$, the model water vapor is expected to be decreased accordingly. It is obvious that the scheme does not provide an proportional relationship between Δq_v and Δq_r. For example, for $\Delta q_r > 0$, when the rain water increments were 0.5×10^{-4} kg kg^{-1}, the corresponding water vapor increments were approximately 1.0×10^{-3} kg kg^{-1} on average, while for $\Delta q_r < 0$, the water vapor decreased by around 0.5×10^{-3} kg kg^{-1} corresponding to the -0.5×10^{-4} kg kg^{-1} of rain water increments. Moreover, apparently, if there is no minimization operator used in Eq. (9), the scheme might provide increased water vapor increments even when the negative rain water increments were given, which shows that the model back-

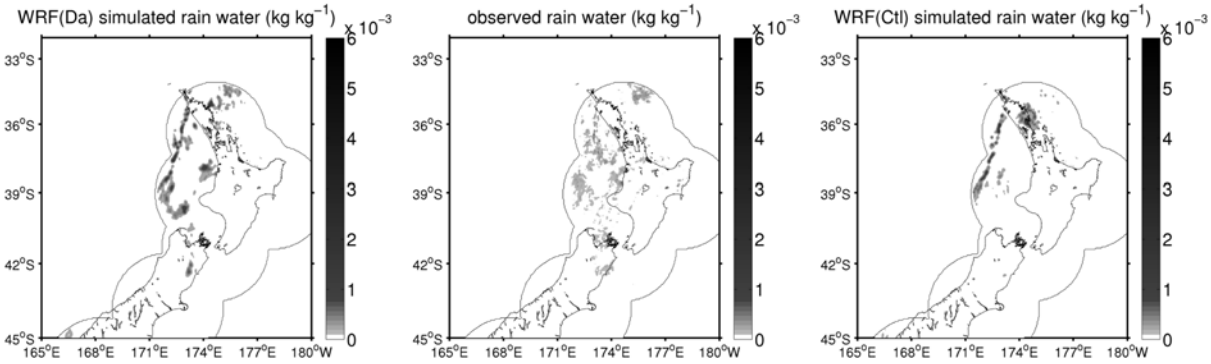

Fig. 12. The simulated maximum rain water in a column for the Da run (bottom-left) and the Ctl run (bottom-right) and the associated radar derived rain water (top) at 0100 UTC 1 November 2011 (threshold: 0.2×10^{-3} kg kg^{-1}).

ground fields might not be well in agreement with the reverse Kessler scheme at all grid points if the model precipitation is overestimated.

The WRF simulated maximum rain water in a volume for both the Da run and Ctl run and the associated radar derived rain water at 0100 UTC (30 min after the time window) were also presented in Fig. 12. The relationship between radar observed reflectivity and rain water is given by Eq. (1). It is apparent that, compared to the Ctl run, the rain water produced by the Da run is closer to the actual observation, although both simulations missed several observed rain water in the west coast of the North Island. The spurious rain water produced by the Ctl run in the Northland region has been eliminated by the nudging processes. The simulated rain water for both experiments usually showed similar magnitude compared to the observation on average but higher intensity can be found in some regions than the observed one, which is agreement with the subjective evaluations and the analysis presented in Fig. 8-10 before.

4. Discussions

Considering the computing resources available for research applications in New Zealand, we conclude they are inadequate for 4D-Var radar assimilation at the present time, the RK-nudging scheme was not only capable of providing better background precipitation related backgrounds, but also required less computational resources. In contrast, the 3D-Var system might lead to segmentation fault or longer adjustment time (usually > 30 min) under current cluster configurations provided by New Zealand eScience Infrastructure (NeSI). It makes the RK-nudging scheme an effective method showing the potential to be used in the New Zealand future rapid update system.

Although the improvements produced by the RK-nudging scheme are scored by both subjective and objective evaluation schemes in the selected events, it is still necessary to mention the potential limitations of the scheme developed. One of the most potentially serious limitations of the RK-nudging scheme comes from the use of the simple Kessler warm rain scheme, which is a liquid only scheme and does not include ice-phase changes. This issue becomes more significant as the time window increases, as Wang *et al*. (2013b) showed a simple liquid only microphysics scheme is an acceptable substitute for the more complex, multi-phases ones only if the time window is short enough (e.g., less than 1 hour). But it is still worth noting that, the essential feature of the Kessler scheme is that it simply separates liquid into cloud water and rainwater based on the Marshall-Palmer distribution for rain. For heavy rainfall which is produced by cold cloud processes, even when we adopt the time window less than 1 hour, the use of a warm rain processes in data assimilation may still well lead to uncertainties in the production of the "correct" partition increments. However, considering the complexity of the inclusion of ice-particle microphysics into model (e.g., the different types of ice like small ice, snow and hail, and a great variety of particle sizes and shapes), currently the reflectivity based operators for most data assimilation systems were still developed according to the liquid only schemes (e.g., Sun and Wang, 2013; and Wang *et al*., 2013b).

On the other hand, even we assume that the use of simple liquid based scheme is acceptable, the empirical relationship based Kessler warm rain precipitation scheme still could have significant errors (e.g., Seifert and Beheng, 2001; Rognvaldsson, 2012). Moreover, oversaturation is not allowed in the RK-nudging which could cause precipitation to be overestimated compared to the associated observation. Thus, a more complicated and accurate microphysics scheme is expected to be employed in radar reflectivity data assimilation in the future.

It is worth noting that, In this paper, there are 13 cases involved in the assimilation experiments, and the precipitation forecasts of most of the cases were improved by the RK-nudging method, but it is still not able to provide a full evaluation of the RK-nudging assimilation over all synoptic characteristics, precipitation features and model backgrounds, especially when we consider the number of samples of each type would be decreased dramatically as the verification threshold increases. In order to do that, a longer period of continuous evaluation (1-3 years) with exactly same operational model configurations (e.g., at current stage, the assimilation with synoptic observations is already implemented in the MetSer-

vice system) is expected to be carried out in the future when stable computational resources are available.

5. Conclusions

This paper described a simple approach to incorporate radar reflectivity into WRF whilst avoiding expensive computational resources, which is essential in New Zealand or other similar countries that is using WRF but will not have large high efficient cluster in the near future. By the use of the reversed Kessler warm rain scheme and relevant saturation adjustments, the radar rainfall estimates can be assimilated into WRF. Reflectivity derived rain water has been converted to associated water vapor then nudging approach was used to assimilate the water vapor and adjust the model moisture fields accordingly. The analyses of the RK-nudging approach were only considering three variables (rain water, cloud water and water vapor) during the nudging processes while other moisture related variables, like potential temperature, pressure etc., were adopted from the model backgrounds. This approach is easily implemented and does not require large computational resources.

A total of 13 cases with significant rainfall occurred in the 2011/2012 summer of New Zealand have been employed to investigate the RK-nudging scheme. Reflectivity observed by NZ MetService radars was incorporated into the model and initialized the model with previous 6 h forecasts. Different forecast skill scores (ETS, FAR and FSS) were used to show the skill changes resulting from the assimilation processes. The results showed that, the RK-nudging scheme was able to improve the forecasts on average up to several hours depending on the verification threshold set (e.g., from FSS, 5 hours for the threshold of 5.0 mm h^{-1} and 6 hours for the threshold of 0.5 mm h^{-1}). However, the improvements produced by the nudging processes decreased rapidly with the verification threshold or forecast lead hours increasing. An example of subjective examination for the case of 1 November 2011 was presented and the results showed that the RK-nudging scheme was capable of adjusting moisture and thus promoting the precipitation forecasts in the radar covered regions on average. In this case, the RK-nudging was able to provide better adjustments in predicting rainfall location rather than the intensity. Moreover, the scheme performs better at increasing the rain area than reducing the incorrectly predicted precipitation areas. The improvements resulting from the assimilation in this case also decreased with the lead hours increasing, and after about 6 hours the improvements introduced by the assimilation became trivial.

In order to develop effective and economic radar reflectivity assimilation scheme(s) for New Zealand, the RK-nudging is expected to be implemented together with other reflectivity nudging approaches (e.g., WVC technique) in WRF. The comparisons between nudging and the more advanced 4D-Var method (Sun and Wang, 2013; Wang *et al*., 2013b) will also be carried out in New Zealand depending on the improved availability of computational resources in the future.

Acknowledgments. This research is funded by the New Zealand National Institute of Water and Atmosphere Research (NIWA). The high-performance computing facilities are provided by the New Zealand eScience Infrastructure (NeSI) and the Centre for eResearch at the University of Auckland, New Zealand. We thank scientists from New Zealand MetService Ltd. for useful discussion about the research project. The authors also wish to thank the anonymous reviewers for their useful comments.

Edited by: Song-You Hong, Kim and Yeh

REFERENCES

Barker, D. M., W. Huang, Y.-R. Guo, and Q. N. Xiao, 2004: A three-dimensional (3DVAR) data assimilation system for use with MM5: implementation and initial results. *Mon. Wea. Rev.,* **132**, 897-914.

_____, and Coauthors, 2012: The weather research and forecasting model's community variational/ensemble data assimilation system: WRFDA. *Bull. Amer. Meteor. Soc.*, **93**, 831-843.

Caya, A., J. Sun, and C. Snyder, 2005: A comparison between the 4D-Var and the ensemble Kalman filter techniques for radar data assimilation. *Mon. Wea. Rev.,* **133**, 3081-3094.

Crouch, J., 2003: Using radar to diagnose weather systems. *Tephra*, 46-48.

Dance, S. L., 2004: Issues in high resolution limited area data assimilation for quantitative precipitation forecasting. *Physica D: Nonlinear Phenomena*, **196(1-2)**, 1-27.

Davolio, S., and A. Buzzi, 2004: A nudging scheme for the assimilation of precipitation data into a mesoscale model. *Wea. Forecasting*, **19**, 855-871.

Dixon, M., Z. Li, H. Lean, N. Roberts, and S. Ballard, 2009: Impact of data assimilation on forecasting convection over the United Kingdom using a high-resolution version of the Met office unified model. *Mon. Wea. Rev.*, **137**, 1562-1584.

Dudhia, J., 1989: Numerical study of convection observed during the winter monsoon experiment using a mesoscale two-dimensional model. *J. Atmos. Sci.,* **46**, 3077-3107.

Gilleland, E., D. A. Ahijevych, B. G. Brown, and E. E. Ebert, 2010: Verifying forecasts spatially. *Bull. Amer. Meteor. Soc.*, **91**, 1365-1373.

Fabry F., A. Bellon, M. Duncan, and G. L. Austin, 1994: High resolution rainfall measurements by radar for very small basins: the sampling problem reexamined. *J. Hydrol.,* **161**, 415-428.

Haase, G., S. Crewell, C. Simmer, and W. Wergen, 2000: Assimilation of radar data in mesoscale models: Physical initialization and latent heat nudging. *Phys. Chem. Earth*, **25**, 1237-1242.

Hagen, M., and S. A. Yuter, 2003: Relations between radar reectivity, liquidwater content, and rainfall rate during the MAP SOP. *Quart. J. Roy. Meteor. Soc*., **129**, 477-493.

Huang, X.-Y., and Coauthors, 2009: Four-dimensional variational data assimilation for WRF: Formulation and preliminary results. *Mon. Wea. Rev.,* **137**, 299-314.

Jones, C. D., and B. Macpherson, 1997: A latent heat nudging scheme for the assimilation of precipitation data into an operational mesoscale model. *Meteor. App1.,* **4**, 269-277.

Kessler, E., 1969: On distribution and continuity of water substance in atmospheric circulations. *Atmos. Res.,* **10**: 32-84.

Klemp, J. B., and R. B. Wilhelmson, 1978: The simulation of three-dimensional convective storm dynamics. *J. Atmos. Sci.*, **35**, 1070-1096.

Krishnamurti, T. N., J. Xue, H. S. Bedi, K. Ingles, and D. Oosterhof, 1991: Physical initialisation for numerical weather prediction over the tropics.

Tellus, **43AB**, 53-81.

Lau K. M., and H. T. Wu, 2003: Warm rain processes over tropical oceans and climate implications. *Geophys. Res. Lett*., **30**, 2290.

Liu, Y., A. Bourgeois, T. Warner, S. Swerdlin, and J. Hacker, 2005: An implementation of obs-nudging-based FDDA into WRF for supporting ATEC test operations. 2005 WRF user workshop. Paper 10.7.

Manobianco, J., S. Koch, V. M. Karyampudi, and A. J. Negri, 1994: The impact of assimilating satellite-derived precipitation rates on numerical simulation of ERICA IOP 4 cyclone. *Mon. Wea. Rev.,* **122**, 341-365.

Mlawer, E. J., S. J. Taubman, P. D. Brown, M. J. Iacono, and S. A. Clough, 1997: Radiative transfer for inhomogeneous atmosphere: RRTM, a validated correlated-k model for the longwave. *J. Geophys. Res.,* **102**, 16663-16682.

Noh, Y., W. G. Cheon, S. Y. Hong, and S. Raasch, 2003: Improvement of the K-profile model for the planetary boundary layer based on large eddy simulation data. *Bound.-Layer Meteor*., **107**, 421-427.

Nunes, A. M. B., and S. Cocke, 2004: Implementing a physical initialization procedure in a regional spectral model: impact on the short-range rainfall forecasting over South America. *Tellus*, **56A(2)**, 125-146.

Ogura, Y., and T. Takahash, 1973: The Development of Warm Rain in a Cumulus Model. *J. Atmos. Sci.*, **30**, 262-277.

Roberts, N. M., and H. W. Lean, 2008: Scale-selective verification of rainfall accumulations from high-resolution forecasts of convective events. *Mon. Wea. Rev.*, **136**, 78-97.

Rognvaldsson O., 2013: Numerical simulations of surface winds and precipitation in Iceland. Ph. D. Thesis, The University of Bergen, 44 pp.

Rossa, A., P. Nurmi, and E. Ebert, 2008: Overview of methods for the verification of quantitative precipitation forecasts. *Precipitation: Advances in Measurement, Estimation and Prediction*. Springer, 417-450 pp.

Schultz, P., 1995: An explicit cloud physics parameterization for operational numerical weather prediction. *Mon. Wea. Rev.*, **123**, 3331-3343.

Seifert, A., and K. D. Beheng, 2001: A double-moment parameterization for simulating autoconversion, accretion and selfcollection. *Atmos. Res*., **59-60**, 265-281.

Snyder, C., and F. Zhang, 2003: Assimilation of simulated Doppler radar observations with an ensemble Kalman filter. *Mon. Wea. Rev.* **131**, 1663-1677.

Stauffer, D. R., and N. L. Seaman, 1990: Use of four-dimensional data assimilation in a limited-area mesoscale model. Part 1: Experiments with synoptic-scale data. *Mon. Wea. Rev.,* **118**, 1250-1277.

_____, and N. L. Seaman, 1994: Multi-scale four dimensional data assimilation. *J. Appl. Meteor. Climatol.,* **33**, 416-434.

Stephan K., S. Klink, and C. Schra, 2008: Assimilation of radar derived rain rates into the convective scale model COSMO-DE at DWD. *Quart. J. Roy. Meteor. Soc.,* **134**, 1315-1326.

Sokol Z., 2009: Effects of an assimilation of radar and satellite data on a very-short range forecast of heavy convective rainfalls. *Atmos. Res.,* **93**, 188-206.

_____, and P. Zacharov, 2012: Nowcasting of precipitation by an NWP model using assimilation of extrapolated radar reectivity. *Quart. J. Roy. Meteor. Soc.,* **138**, 1072-1082.

_____, and D. Rezacova, 2009: Assimilation of the radar-derived water vapour mixing ratio into the LM COSMO model with a high horizontal resolution. *Atmos. Res*., **92**, 331-342.

Soong, S. T., and Y. Ogura, 1973: A comparison between axisymmetric and slab-symmetric cumulus cloud models. *J. Atmos. Sci.*, **30**, 879-893.

Shucksmith, P. E., L. Sutherland-Stacey, and G. L. Austin, 2011: The spatial and temporal sampling errors inherent in low resolution radar estimates of rainfall. *Meteor. Appl.,* **18**, 354-360.

Sun, J., and N. A. Crook, 1997: Dynamical and microphysical retrieval from Doppler radar observations using a cloud model and its adjoint. Part I: Model development and simulated data experiments. *J. Atmos. Sci*., **54**, 1642-1661.

_____, 2005: Convective-scale assimilation of radar data: Progress and challenges. *Quart. J. Roy. Meteor. Soc*., **131**, 3439-3463.

_____, and H. Wang, 2013: Radar data assimilation with WRF 4D-Var. Part II: Comparison with 3D-Var for a squall line over the U.S. great plains. *Mon. Wea. Rev.*, **141**, 2245-2264.

Wang, H., J. Sun, S. Fan, and X. Huang, 2013a: Indirect assimilation of radar reflectivity with WRF 3D-Var and its impact on prediction of four summertime convective events. *J. Appl. Meteor. Climatol.*, **52**, 889-902.

_____, J. Sun, X. Zhang, X. Huang, and T. Auligné, 2013b: Radar data assimilation with WRF 4D-Var. Part I: System development and preliminary testing. *Mon. Wea. Rev.*, **141**, 2224-2244.

Xiao, Q., Y.-H. Kuo, J. Sun, W.-C. Lee, D. M. Barker, and E. Lim, 2007: An approach of radar reflectivity data assimilation and its assessment with the Inland QPF of Typhoon Rusa (2002) at landfall. *J. Appl. Meteor. Climatol*., **46**, 14-22.

_____, _____, _____, _____, E. Lim,Y.-R. Guo, and D. M. Barker, 2005: Assimilation of Doppler radar observations with a regional 3D-Var system: Impact of Doppler velocities on forecasts of a heavy rainfall case. *J. Appl. Meteor. Climatol*., **44**, 768-788.

Yang, Y., C. Qiu, and J. Gong, 2006: Physical initialization applied in WRF-Var for assimilation of Doppler radar data. *Geophys. Res. Lett*., **33**, LL22807.

Zhang, F., C. Snyder, and J. Sun, 2004: Impacts of initial estimate and observations on convective-scale data assimilations. *Mon. Wea. Rev*., **132**, 1238-1253.